www.czasopisma.pan.pl PAN www.journals.pan.pl

Metrol. Meas. Syst., Vol. XVIII (2011), No. 3, pp. 391-402.

METROLOGY AND MEASUREMENT SYSTEMS

Index 330930, ISSN 0860-8229

www.metrology.pg.gda.pl

MINIMIZATION OF MAXIMUM ERRORS IN UNIVERSAL APPROXIMATION OF THE UNIT CIRCLE BY A POLYGON

Józef Borkowski

Wroclaw University of Technology, Chair of Electronic and Photonic Metrology, ul. B. Prusa 53/55, 50-317 Wroclaw, Poland (✉Jozef.Borkowski@pwr.wroc.pl)

Abstract

This paper presents a universal approximation of the unit circle by a polygon that can be used in signal processing algorithms. Optimal choice of the values of three parameters of this approximation allows one to obtain a high accuracy of approximation. The approximation described in the paper has a universal character and can be used in many signal processing algorithms, such as DFT, that use the mathematical form of the unit circle. One of the applications of the described approximation is the DFT linear interpolation method (LIDFT). Applying the results of the presented paper to improve the LIDFT method allows one to significantly decrease the errors in estimating the amplitudes and frequencies of multifrequency signal components. The paper presents the derived formulas, an analysis of the approximation accuracy and the region of best values for the approximation parameters.

Keywords: Unit circle, approximation by polygon, LIDFT, interpolated DFT, zero padding.

1. Introduction: spectral analysis and the unit circle approximation

There are many methods applicable to spectral analysis for estimating the amplitudes, frequencies and phases of component oscillations in a multifrequency waveform. A set of these methods covers procedures generally based on the Prony method and correlation methods founded on properties of the signal autocorrelation matrix [1-5]. However, problems with complicated and nonlinear procedures for estimating component frequencies must then be addressed. As an example, in the least squares Prony method, the component frequencies are determined from the locations of zeros in a high-order polynomial. The other group of spectral analysis methods determines the local maxima of the spectrum, while the locations (on the frequency axis) and the values (on the amplitude and phase axis) of these maxima determine the parameters of the component oscillations. Determining the frequencies, i.e., the locations of local maxima of the spectrum, is the most difficult problem in these methods. For this purpose, iterative algorithms have been applied [6-10], the nonparametric spectrum interpolation methods [11-12] are applicable (zero padding technique [13], chirped-Z transform [14-17], warped DFT [18-20] and interpolation by decimation [11]) and the methods of interpolated DFTs have been developed [21-46]. Nonparametric spectrum interpolation methods make it possible to zoom in on the frequency domain but do not decrease the errors caused by long-range spectral leakage (i.e., by sidelobes of spectrum lines of neighbor components in the spectrum), which are defined by the frequency characteristic of the data window applied [47]. Similarly, the long-range spectral leakage is neglected in all noniterative interpolated DFT methods, except the DFT linear interpolation method (LIDFT) [33-35, 45] and the multipoint weighted interpolated DFT (MWIDFT) method [36, 38, 43]. However, the MWIDFT method is defined only for some classes of cosine-family data windows, i.e., for the class I of Rife-Vincent windows [21], also called the maximum sidelobe

Article history: received on June 1, 2011; accepted on June 17, 2011; available online on Sep. 26, 2011; DOI: 10.2478/v10178-011-0006-x.

decay windows [38, 41, 43]. Some of the interpolated DFT methods are applied only for the rectangular data window, for which errors caused by long-range spectral leakage are the highest [28-30], and some of these interpolations are proposed only for others specific data windows [21, 23-27, 39, 44, 46]. The interpolated DFT methods are the most important methods for the subject of the present paper because one of these methods, the LIDFT method, uses the approximation of the unit circle by a polygon. This approximation is treated here as a separate problem because of the possibility of applying it in other DSP algorithms. Based on the use of the unit circle approximation in the LIDFT method, it can be concluded that the goals of approximating the unit circle with a polygon are as follows:

- linearizing relationships to determine component frequencies (by linearizing the nonlinear shape of the circle by a piecewise-linear shape).
- decreasing the influence of spectrum leakage (by approximation of the data window frequency characteristic, i.e., spectral leakage, by linear functions).
- obtaining solutions for a wide class of data windows (because the approximation of the unit circle by a polygon is independent of the data window used).

In comparison with chirp-Z application in the spectral analysis (which also uses a kind of approximation of the unit circle), the essential difference is visible. In the chirp-Z transform, the approximation of part of the unit circle by a spiral arc only allows zooming in the frequency domain but does not decrease the errors caused by long-range spectral leakage and does not eliminate the nonlinearity of the estimating problem. The LIDFT method does decrease the errors caused by spectral leakage, and it does linearize the equations. Therefore, the approximation of the unit circle by a polygon has the unique property of being able to improve the DSP algorithm, regardless of whether floating-point or fixed-point arithmetic is used.

The approximation of the unit circle by a polygon in the LIDFT method is generalized in the present paper to the much more universal and optimal form, which can be used in many other DSP algorithms. The paper is organized as follows. Section 2 defines the approximation of the arc segment by a line segment and minimizes the approximation errors through the choice of the approximation parameters. Section 3 defines the approximation of the unit circle based on the arc approximation from Section 2. Section 4 includes general remarks and describes the results of using the presented approximation in the LIDFT method.

2. Approximation of the arc by a line

Let us define the following for the unit circle:

$$W_N^{n\lambda} = e^{-j2\pi n\lambda/N} \tag{1}$$

and the circular arc segment:

$$W_M^{n\gamma} = e^{-j2\pi n\gamma/M},\ \gamma \in [-1/2, 1/2],\ M = NR, \tag{2}$$

which is the part of the unit circle (1) for $\lambda \in [-0.5/R, 0.5/R]$, i.e., this arc is appointed by the angle $x_n = \pi n/M$ (Fig. 1a). Let us also define the approximation of this arc by the following line segment (Fig. 1a):

$$\hat{W}_M^{n\gamma} = \alpha_n + j\gamma\beta_n,\ \gamma \in [-1/2, 1/2], \tag{3}$$

where α_n and β_n are defined with parameters η_1 and η_2 based on trigonometric formulas for the angle x_n (Fig. 1b):

$$\alpha_n(\eta_1) = (1-\eta_1)\cos x_n + \eta_1,\ \eta_1 \in [0, 1], \tag{4}$$

$$\beta_n(\eta_2) = -2\cdot[(1-\eta_2)\sin x_n + \eta_2 \tan x_n],\ \eta_2 \le \eta_1. \tag{5}$$

Metrol. Meas. Syst., Vol. XVIII (2011), No. 3, pp. 391-402.

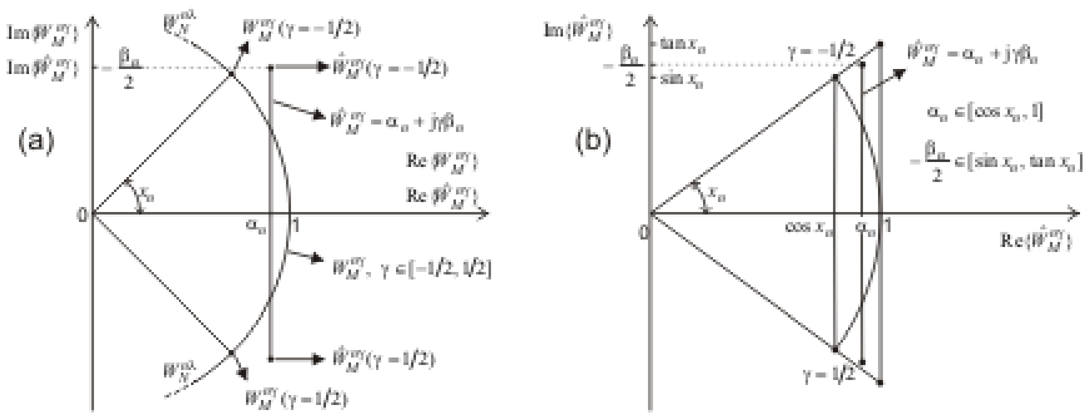

Fig. 1. (a) Approximation of the part ($W_M^{n\gamma}$) of the unit circle ($W_N^{n\lambda}$) by the line segment $\hat{W}_M^{n\gamma} = \alpha_n + j\gamma\beta_n$, (b) definition of the approximated arc segment by a line, acc. to Eqs. (4)–(5).

The optimal choice of the η_1 and η_2 values is based on the minimization of the approximation error ($\hat{W}_M^{n\gamma} - W_M^{n\gamma}$)—its real and imaginary part—and also on the difference between the arguments $\hat{W}_M^{n\gamma}$ and $W_M^{n\gamma}$:

$$\Delta_r(\gamma) = \mathrm{Re}\{\hat{W}_M^{n\gamma} - W_M^{n\gamma}\} = \alpha_n - \cos 2\gamma x_n, \tag{6}$$

$$\Delta_i(\gamma) = \mathrm{Im}\{\hat{W}_M^{n\gamma} - W_M^{n\gamma}\} = \gamma\beta_n + \sin 2\gamma x_n, \tag{7}$$

$$\Delta_a(\gamma) = \arg\{\hat{W}_M^{n\gamma}\} - \arg\{W_M^{n\gamma}\} = 2\gamma x_n + \arctan\frac{\gamma\beta_n}{\alpha_n}. \tag{8}$$

Taking into account (4)–(8), it can be seen that $\Delta_r(\gamma)$ depends on η_1, $\Delta_i(\gamma)$ depends on η_2 and $\Delta_a(\gamma)$ depends on both η_1 and η_2. For all of these errors, the coefficients $k_r(\eta_1)$, $k_i(\eta_2)$ and $k_a(\eta_1,\eta_2)$ are defined as:

$$k_r(\eta_1) = \frac{\max_\gamma |\Delta_r(\gamma)|}{\min_{\eta_1}\{\max_\gamma |\Delta_r(\gamma)|\}}, \tag{9}$$

$$k_i(\eta_2) = \frac{\max_\gamma |\Delta_i(\gamma)|}{\min_{\eta_2}\{\max_\gamma |\Delta_i(\gamma)|\}}, \tag{10}$$

$$k_a(\eta_1,\eta_2) = \frac{\max_\gamma |\Delta_a(\gamma)|}{\min_{\eta_1,\eta_2}\{\max_\gamma |\Delta_a(\gamma)|\}}. \tag{11}$$

The goal of minimizing the maxima of errors (6)–(8) is to find values of η_1 and η_2 that minimize $\max_\gamma |\Delta_r(\gamma)|$, $\max_\gamma |\Delta_i(\gamma)|$ and $\max_\gamma |\Delta_a(\gamma)|$, i.e., values for which (9)–(11) are equal to 1. The minimization is done by equating the first derivatives (with respect to γ) of (6)–(8) to zero, controlling the sign of the second derivatives and, after finding the extremes of (6)–(8), choosing values of η_1 and η_2 that minimize the modulus of (6)–(8) for $x_n << 1$ and $\gamma \in [-1/2, 1/2]$. Such minimization takes into account the dynamic of the moving points, which plots the shape of the arc and the line segments when γ changes, because it takes into account all possible values of the errors for all γ from the range $\gamma \in [-1/2, 1/2]$. The details of these minimizations are included in Appendices A–C.

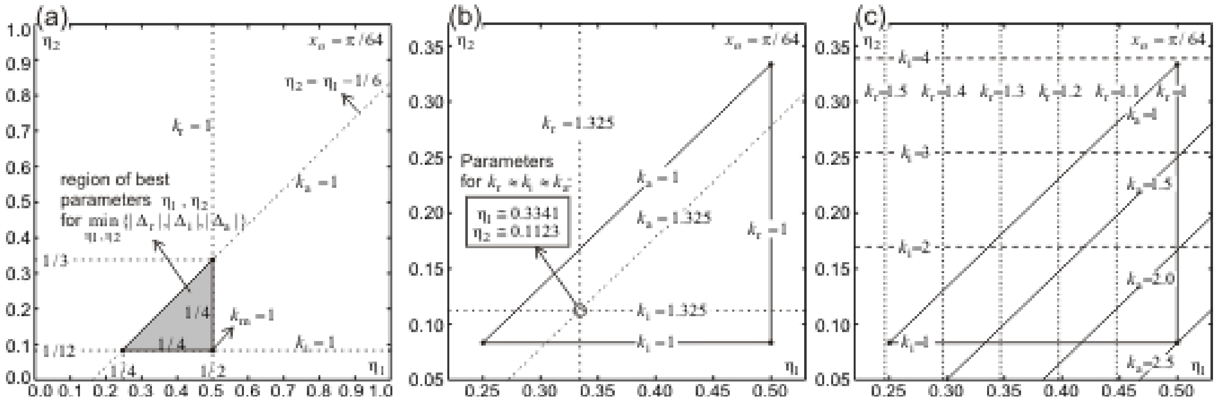

Fig. 2. (a) The region of best values for the approximation parameters η_1 and η_2, (b) the case of the simultaneous increase of k_r, k_i and k_a: $\eta_1 \cong 0.3341$ and $\eta_2 \cong 0.1123$, (c) the contour plot of k_r, k_i, k_a as a function of η_1 and η_2 within the triangle of the best parameters.

The value $\eta_1 = 1/2$ minimizes $\max_\gamma |\Delta_r(\gamma)|$, i.e., $k_r(\eta_1 = 1/2) = 1$ (App. A); the value $\eta_2 = 1/12$ minimizes $\max_\gamma |\Delta_i(\gamma)|$, i.e. $k_i(\eta_2 = 1/12) = 1$ (App. B); and condition $\eta_1 - \eta_2 = 1/6$ minimizes $\max_\gamma |\Delta_a(\gamma)|$, i.e., $k_a(\eta_1, \eta_2) = 1$ for all η_1 and η_2 that fulfilled this condition (App. C). These three conditions ($\eta_1 = 1/2$, $\eta_2 = 1/12$, $\eta_1 - \eta_2 = 1/6$) make the triangle on the plane (η_1, η_2), as is shown on Fig. 2a. This means that it is not possible to fulfill all three conditions concurrently, and it is necessary to choose values of η_1 and η_2 from the region of the best parameters shown in Fig. 2a. For example, if we want to increase all maxima of errors (6)–(8) to the same degree, we should take $\eta_1 \cong 0.3341$ and $\eta_2 \cong 0.1123$. Then, all coefficients (9)–(11) are equal to ca. 1.325 (Fig. 2b). For other additional criteria, the contour plot from Fig. 2c is useful.

Based on these results, the approximation of the whole unit circle is defined in Section 3.

3. Approximation of the unit circle by a polygon

After rotating the line segment (3) by the angle $-2kx_n$ (i.e., multiplying by e^{-j2kx_n}) or by the angle $-2(k \pm 1/2)x_n$ (i.e., multiplying by $e^{-j2(k\pm 1/2)x_n}$), the rest of the parts of the unit circle are obtained for integer values of k: for $\lambda_k \in [(k-0.5)/R, (k+0.5)/R]$, Fig. 3a; for $\lambda_k \in [k/R, (k+1)/R]$, Fig. 3b; and for $\lambda_k \in [(k-1)/R, k/R]$, Fig. 3c:

$$e^{-j2\pi n\lambda_k/N} \approx e^{-j2\pi nk/M}[\alpha_n + j\gamma_k\beta_n],\ \lambda_k = \frac{1}{R}(k + \gamma_k),\ \gamma_k \in [-1/2, 1/2], \tag{12}$$

$$e^{-j2\pi n\lambda_k/N} \approx e^{-j2\pi nk/M}e^{-jx_n}[\alpha_n + j\gamma_k\beta_n],\ \lambda_k = \frac{1}{R}(k + \frac{1}{2} + \gamma_k),\ \gamma_k \in [-1/2, 1/2], \tag{13}$$

$$e^{-j2\pi n\lambda_k/N} \approx e^{-j2\pi nk/M}e^{jx_n}[\alpha_n + j\gamma_k\beta_n],\ \lambda_k = \frac{1}{R}(k - \frac{1}{2} + \gamma_k),\ \gamma_k \in [-1/2, 1/2]. \tag{14}$$

For $\eta_2 < \eta_1$, the approximation polygon has a discontinuity, and the degree of this discontinuity depends on the value of $\eta_1 - \eta_2$ (Fig. 4a). The approximation error for a given value of n, N, η_1 and η_2 can be reduced with increasing R, which results in an increase in the number of approximated polygon sides (Fig. 4b).

Metrol. Meas. Syst., Vol. XVIII (2011), No. 3, pp. 391-402.

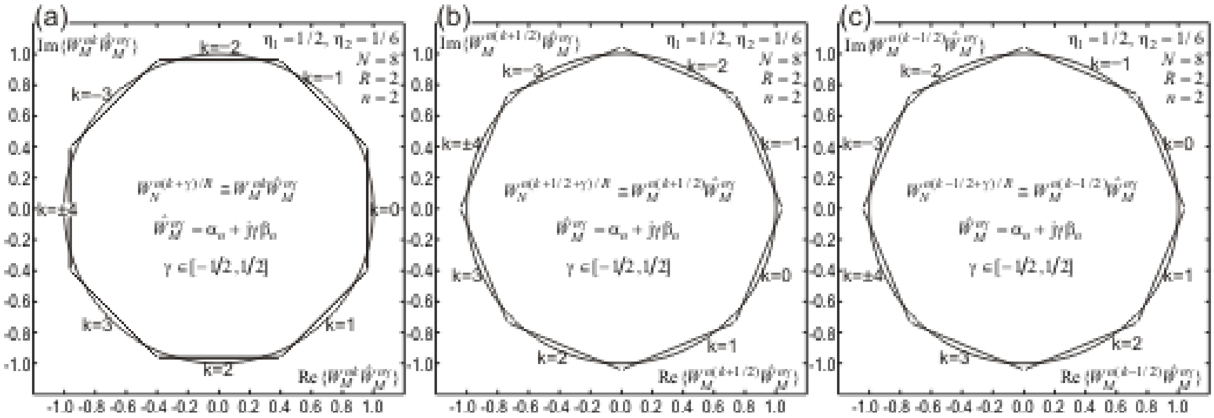

Fig. 3. Approximation of the unit circle, acc. to Eqs. (12)–(14), as the effect of approximation of an arc segment by a line segment and its rotation by the angle $-2kx_n$ or $-2(k\pm 1/2)x_n$, i.e., multiplying by (a) e^{-j2kx_n} or (b, c) $e^{-j2(k\pm 1/2)x_n}$.

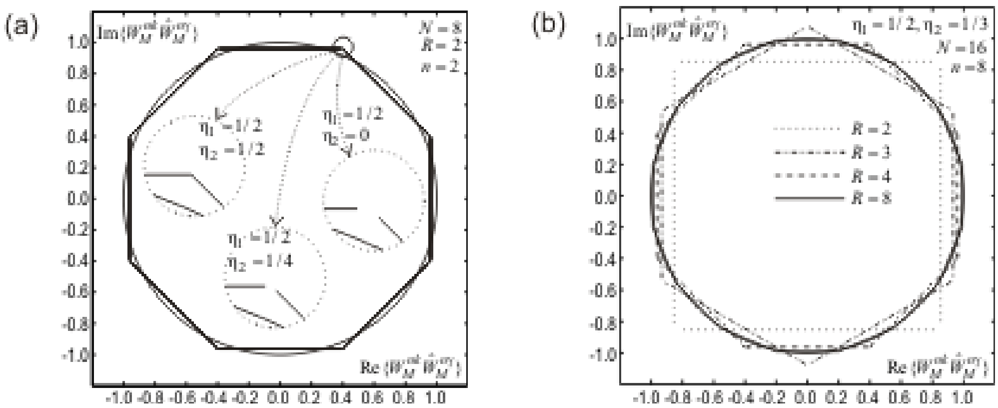

Fig. 4. (a) The influence of η_1 and η_2 on the discontinuity of the approximation polygon, acc. to Eq. (12), for three cases: (η_1,η_2) = (1/2, 1/2), (1/2, 1/4), (1/2, 0) – the example is for n = 2, N = 8 and R = 2, (b) the effect of decreasing the error of approximating the unit circle with a polygon by increasing R (the example is for n = 8, N = 16, η_1 = 1/2 and η_1 = 1/3).

Most often, as in DFT, DSP algorithms use the values $W_N^{n\lambda}$ for all n from the range $n \in [-N/2, N/2-1]$. This means, taking into account the fact that $M = NR$, that $x_n = n\pi/M$ varies in the range $x_n \in [-\pi/(2R), \pi/(2R))$. The biggest error in the approximation of the unit circle by a polygon appears for cases of big values of n close to $\pm N/2$ (Fig. 5), but the influence of these cases is limited in practice by applying data windows other than the rectangular window [47], which have values close to zero for n close to $\pm N/2$. If necessary, the approximation error can be reduced by increasing R, which means, in practice, increasing the number of padded zeros in the zero padding technique. For n of the form $n = \pm 2^m$ (m—natural number) the polygons resulting for successive k from the range $k \in [-M/2, M/2-1]$ overlap each other, but for $n \neq \pm 2^m$, the polygons are shifted relative to each other (Fig. 5).

4. Conclusions

The main results of the paper are Eqs. (4)–(5) and (12)–(14) with Figs. 2a-2c, which are useful for choosing the parameters η_1 and η_2. Besides these two parameters, the accuracy of the approximation can be increased by the third parameter R, which, when applying the technique to DFT with $R > 1$, means the zero padding technique. The most convenient

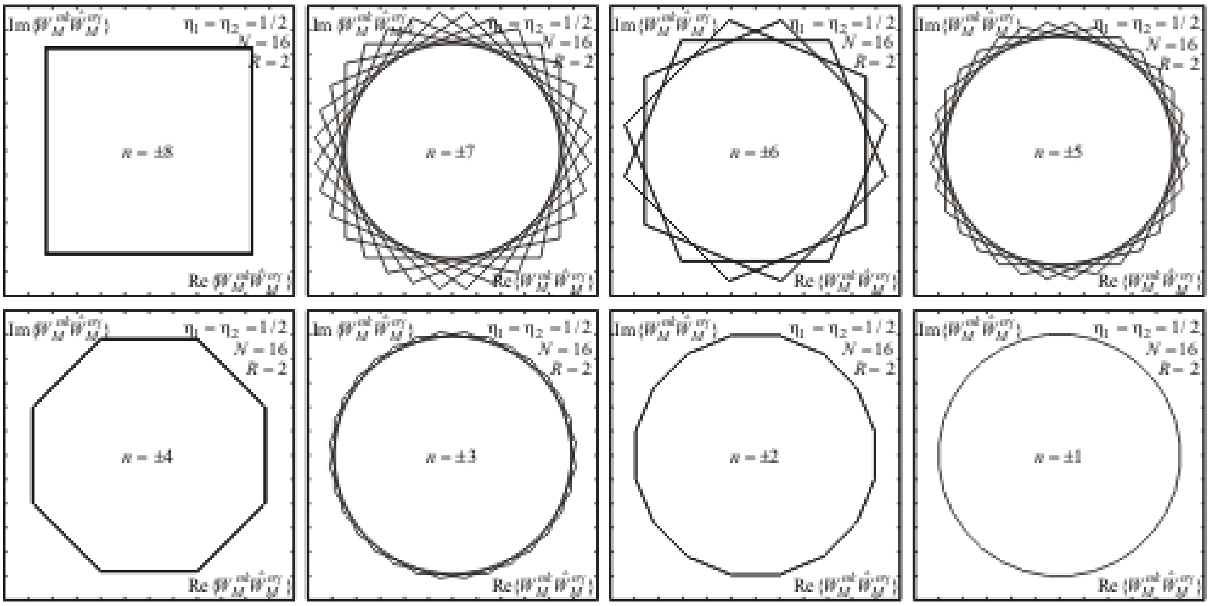

Fig. 5. Approximation of the unit circle by a polygon, acc. to Eq. (12), for $n = -N/2,\ldots,N/2$ (and $k = -NR/2,\ldots$ $\ldots,NR/2-1$ for a given n). The shifting of the polygons is visible for $n \neq \pm 2^m$, and the overlapping of the polygons is visible for $n = \pm 2^m$. The increase in the approximation error is noticeable for increasing $|n|$.

approximation of those given by Eqs. (12)–(14) is Eq. (12) because it does not require multiplying by e^{-jx_n} (as do Eqs. (13)–(14)).

The presented approximation of the unit circle is universal because it can be used in every method that uses a unit circle defined by (1). One of these applications is the DFT linear interpolation method (LIDFT), which originally [33-35, 45] used approximation (14) with the functions $\alpha_n = \operatorname{sinc} x_n$ and $\beta_n = 6(\cos x_n - \operatorname{sinc} x_n)/x_n$. However, when approximation (12) is used instead of this approximation, with α_n and β_n defined by Eqs. (4)–(5), the LIDFT method is more accurate. For the LIDFT method, the values of η_1 and η_2 that are close to optimal are the following: $\eta_1 = 1/2$ and $\eta_2 = 1/6$. For this case, $k_\mathrm{r} = 1$ and $k_\mathrm{i} \cong k_\mathrm{a} \cong 2$. Because of the linearity of (3) with respect to γ, the matrix equation of the LIDFT method is also linear, which is one of the most important advantages of this method. A detailed analysis of the application of the presented universal approximation to the LIDFT method will be the subject of a separate paper. All methods using the described universal approximation of the unit circle by a polygon should choose parameters η_1 and η_2 from the triangle of best parameters from Figs. 2a-2c. The final choice depends on the properties of the applied method. The presented approximation has the potential to solve other estimation problems, such as [48, 49], after the use of approximation methods based on Fourier transform.

Appendix A. Minimization of (6) and (9)

The optimal value of η_1, which minimizes $\max_\gamma |\Delta_\mathrm{r}(\gamma)|$ and $k_\mathrm{r}(\eta_1)$, is obtained from Eqs. (4) and (6) and Fig. 6: $\eta_1 = 1/2$ minimizes $\max_\gamma |\Delta_\mathrm{r}(\gamma)|$. The plots of $\Delta_\mathrm{r}(\gamma)$ versus γ for different values of η_1 (Fig. 7a) confirm this result, and Fig. 7b shows that the optimal value of η_1 does not depend on *n*.

Metrol. Meas. Syst., Vol. XVIII (2011), No. 3, pp. 391-402.

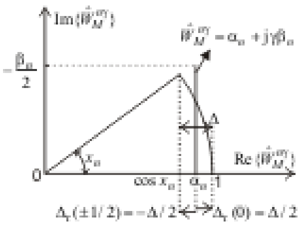

Fig. 6. Minimization of the $\max_\gamma |\Delta_r(\gamma)|$.

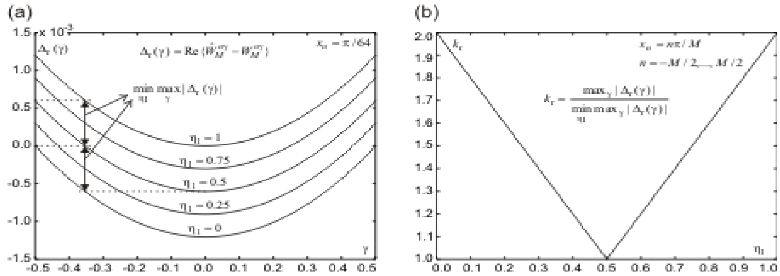

Fig. 7. (a) The error $\Delta_r(\gamma)$ versus γ and the minimization of $\max_\gamma |\Delta_r(\gamma)|$ for $\eta_1 = 1/2$, (b) coefficient k_r versus parameter η_1.

Appendix B. Minimization of (7) and (10)

The first and second derivative of $\Delta_i(\gamma)$ are given by:

$$\frac{d\Delta_i(\gamma)}{d\gamma} = \beta_n + 2x_n \cos 2\gamma x_n , \quad \frac{d^2\Delta_i(\gamma)}{d\gamma^2} = -4x_n^2 \sin 2\gamma x_n \tag{B.1}$$

and the extremes of $\Delta_i(\gamma)$ are given for equating the first derivative to zero (the sign of the second derivative implies that the minimum is for $\gamma x_n < 0$ and the maximum is for $\gamma x_n > 0$):

$$\gamma_0 = \pm(2x_n)^{-1} \arccos[-\beta_n /(2x_n)]. \tag{B.2}$$

From the Maclaurin series of the first derivative (B.1) with respect to x_n, after equating it to zero and assuming $o(x_n^2) = 0$:

$$\gamma_0 \approx \pm\frac{1}{2}\sqrt{\frac{1}{3} - \eta_2} , \; \eta_2 \approx \frac{1}{3} - 4\gamma_0^2 . \tag{B.3}$$

For $\gamma \in [-0.5, 0.5]$, there is $-2/3 \le \eta_2 \le 1/3$. The error $\max_\gamma |\Delta_i(\gamma)|$ achieves a minimum when $y = \Delta_i(\gamma_0) + \Delta_i(-1/2) = 0$ for $\gamma_0 < 0$ (or $y = \Delta_i(\gamma_0) + \Delta_i(1/2)$ for $\gamma_0 > 0$) (Fig. 8a):

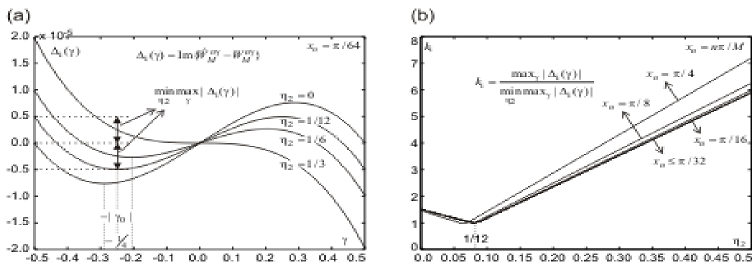

Fig. 8. (a) The error $\Delta_i(\gamma)$ versus γ and the minimization of $\max_\gamma |\Delta_i(\gamma)|$ for $\eta_2 = 1/12$, (b) coefficient k_i versus η_2 and the shifting minimum for $|x_n| > \pi/32$.

$$y = \gamma_0 \beta_n + \sin 2\gamma_0 x_n - \frac{\beta_n}{2} - \sin x_n = 0,\ \gamma_0 = -(2x_n)^{-1} \arccos[-\beta_n /(2x_n)]. \tag{B.4}$$

Applying (5) in (B.4) and expanding y to a Maclaurin series with respect to x_n:

$$y = -\frac{18\eta_2^2 - (12 - 27\sqrt{1/3 - \eta_2})\eta_2 + 2}{54\sqrt{1/3 - \eta_2}} x_n^3 + o(x_n^5) = 0. \tag{B.5}$$

Assuming $o(x_n^5) = 0$, after solving (B.5) with respect to η_2, a double root ($(\eta_2)_1 = -2/3$) and one simple root ($\eta_2 = 1/12$) are obtained. The last equation minimizes $\max_\gamma |\Delta_i(\gamma)|$ and then from (B.3), it is implied that $\gamma_0^2 \approx 1/16$. The double root $(\eta_2)_1 = -2/3$ was excluded because (B.3) implies that $\gamma_0^2 \approx 1/4$. Expanding $\Delta_i(\gamma_0)$ and $\Delta_i(\pm 1/2)$ to the Maclaurin series implies that for this case, $\max_\gamma |\Delta_i(\gamma)|$ is much greater than for $\eta_2 = 1/12$ (Fig. 8a).

Plots of Δ_i, k_i versus γ and η_2 are shown in Fig. 8. Fig. 8b also shows that the optimal value of η_2 is slightly lower than 1/12 (obtained from the assumption that $o(x_n^5) = 0$) for big values of x_n. For values $|x_n| \le \pi/32$, plots $k_i = k_i(\eta_2)$ overlap each other (with an accuracy not smaller than that resulting from the resolution of the graph in Fig. 8b). However, the influence of values $|x_n| > \pi/32$ is reduced in practice by the use of data windows other than rectangular window [47], which have values close to zero for n close to $\pm N/2$.

Appendix C. Minimization of (8) and (11)

For the use of approximations with parameters $\eta_1 = 1/2$ (obtained in App. A) and $\eta_2 = 1/12$ (obtained in App. B), the error of the unit circle argument, defined by (8), depends on γ. Fig. 9 shows this error for $\gamma = 0, -1/8, ..., -1/2$. A similar situation exists for other values of η_1 and η_2. To determine the condition that minimizes $\max_\gamma |\Delta_a(\gamma)|$ and k_a, the analysis is performed in a manner similar to that in App. B.

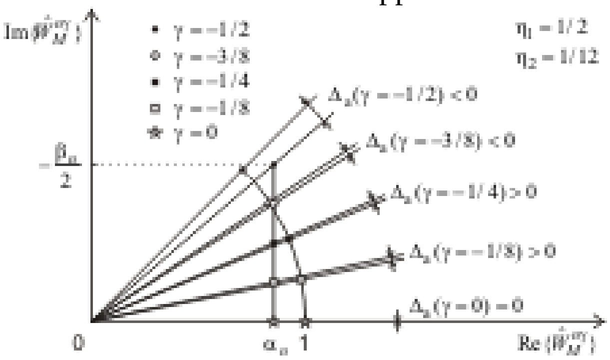

Fig. 9. Definition of the error $\Delta_a(\gamma)$ for chosen values of γ.

The extreme of $\Delta_a(\gamma)$ is given for the condition:

$$\left. \frac{d\Delta_a(\gamma)}{d\gamma} \right|_{\gamma=\gamma_0} = 2x_n + \frac{\beta_n}{\alpha_n} [1 + \gamma_0^2 (\beta_n / \alpha_n)^2]^{-1} = 0, \tag{C.1}$$

i.e.:

Metrol. Meas. Syst., Vol. XVIII (2011), No. 3, pp. 391-402.

$$\gamma_0^2 = -\frac{\alpha_n}{\beta_n}\left(\frac{1}{2x_n} + \frac{\alpha_n}{\beta_n}\right). \tag{C.2}$$

After applying Eqs. (4)–(5) and expanding (C.2) into the Maclaurin series with respect to x_n and assuming $o(x_n^2) = 0$, the following is obtained:

$$\gamma_0 \approx \pm\frac{1}{2}\sqrt{\frac{3\eta_2 - 3\eta_1 + 2}{6}}. \tag{C.3}$$

Minimization of $\max_\gamma |\Delta_a(\gamma)|$ is achieved when $y = \Delta_a(\gamma_0) + \Delta_a(-1/2) = 0$ for $\gamma_0 < 0$ (or $y = \Delta_a(\gamma_0) + \Delta_a(1/2) = 0$ for $\gamma_0 > 0$) (Fig. 10a):

$$y = 2\gamma_0 x_n + \arctan\frac{\gamma_0\beta_n}{\alpha_n} - x_n - \arctan\frac{\beta_n}{2\alpha_n} = 0,\ \gamma_0 = -\sqrt{-\frac{\alpha_n}{\beta_n}\left(\frac{1}{2x_n} + \frac{\alpha_n}{\beta_n}\right)}. \tag{C.4}$$

Applying Eqs. (4)–(5) in (C.4) and expanding y into the Maclaurin series with respect to x_n yields:

$$y = \frac{1}{18}\left[2\sqrt{4/3-2\eta_1+2\eta_2} - \eta_1\left(9+\sqrt{6(2-3\eta_1+3\eta_2)}\right) + \eta_2\left(9+\sqrt{6(2-3\eta_1+3\eta_2)}\right)\right]x_n^3 + o(x_n^5) = 0. \tag{C.5}$$

By assuming $o(x_n^5) = 0$ and solving (C.5) with respect to η_2, the 5 roots of this equation are obtained:

$$(\eta_2)_1 = \eta_1 + 4/3,\ (\eta_2)_2 = \eta_1 - 1/6, \tag{C.6}$$

$$(\eta_2)_3 = \eta_1 + 31/18 - a/18 - 1009/(18a), \tag{C.7}$$

$$(\eta_2)_4 = \eta_1 + 31/18 + ab/36 + 1009c/(36a), \tag{C.8}$$

$$(\eta_2)_5 = \eta_1 + 31/18 + ac/36 + 1009b/(36a), \tag{C.9}$$

$$a = (-31159 + 432j\sqrt{302})^{1/3},\ b = 1 - j\sqrt{3},\ c = 1 + j\sqrt{3}. \tag{C.10}$$

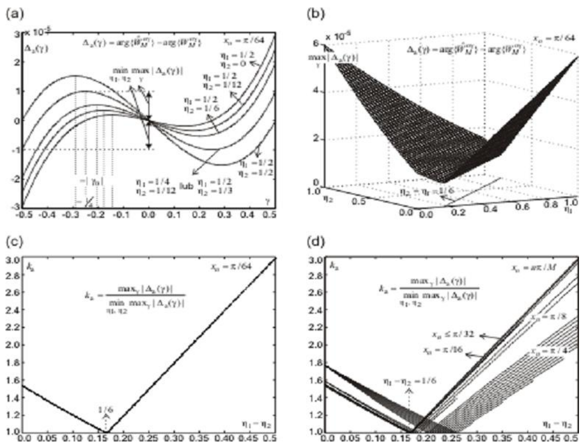

Fig. 10. (a) The error $\Delta_a(\gamma)$ versus γ for chosen values of η_1 and η_2, (b) the error $\max_\gamma |\Delta_a(\gamma)|$ versus parameters η_1 and η_2 for $x_n = \pi/64$, (c) coefficient k_a versus $\eta_1 - \eta_2$ for $x_n = \pi/64$, (d) coefficient k_a versus $\eta_1 - \eta_2$ and the shifting minimum for $|x_n| > \pi/32$.

from which only the first two are real. From the (C.3) condition, $|\gamma_0|=1/2$ is obtained for $(\eta_2)_1$ and $|\gamma_0|\approx 1/4$ is obtained for $(\eta_2)_2$. Taking into account (C.4), minimization of $\max_\gamma |\Delta_a(\gamma)|$ is achieved for $|\gamma_0|\approx 1/4$ (see also Fig. 10a), so the optimal value η_2 corresponds to $(\eta_2)_2$ from (C.6):

$$\eta_2 = \eta_1 - 1/6. \tag{C.11}$$

Example plots of $\Delta_a(\gamma)$ and k_a versus γ and η_1 and η_2 are given in Figs. 10a-10d. The first one illustrates the obtained relationships, especially for the optimal case (of the minimization of $\max_\gamma |\Delta_a(\gamma)|$) that was calculated for various values of η_1 and η_2 (e.g., $\eta_1 = 1/4$, $\eta_2 = 1/12$ or $\eta_1 = 1/2$, $\eta_2 = 1/3$) and that fulfilled condition (C.11). This figure also shows that the maximum of $|\Delta_a(\gamma)|$, under condition (C.11), occurs for $\gamma = \pm 1/2$, and according to (C.3), for $\gamma \approx \pm 1/4$. The plot from Fig. 10b with the line $\eta_2 = \eta_1 - 1/6$ on the contour plot on the plane (η_1, η_2) confirms condition (C.11). The dependence of $\max_\gamma |\Delta_a(\gamma)|$ only on $(\eta_1 - \eta_2)$ means that on the plots of $\max_\gamma |\Delta_a(\gamma)|$ versus $(\eta_1 - \eta_2)$ (which are the set of 2D cuts of the 3D plot from Fig. 10b), all the 2D cuts overlap each other, as is shown for plots of k_a in Fig. 10c.

For small values of x_n (fulfilling the condition $|x_n| \le \pi/32$), condition (C.11) minimizes $\max_\gamma |\Delta_a(\gamma)|$ (with an accuracy not smaller than that resulting from the resolution of the graph in Fig. 10d), but for $|x_n| > \pi/32$, the additional effect in Fig. 10d is noticeable. The 2D cuts of the 3D plot from Fig. 10b do not overlap each other (which means that the function does not only depend on $(\eta_1 - \eta_2)$), and the optimal value of $(\eta_1 - \eta_2)$ is greater than the 1/6 determined by (C.11). However, the influence of $|x_n| > \pi/32$ can be reduced by increasing the parameter R, regardless of the fact that in practice, a data window other than a rectangular window is applied, which reduces the effect of modifying condition (C.11) for $|x_n| > \pi/32$.

References

[1] Marple, S.L. (1987). *Digital Spectral Analysis with Applications*, Prentice-Hall.

[2] Kay, S.M. (1988). *Modern Spectral Estimation: Theory and Application*, Englewood Cliffs, Prentice-Hall.

[3] Scharf, L.L. (1991). *Statistical Signal Processing: Detection, Estimation and Time Series Analysis*, Addison–Wesley.

[4] Mitra, S.K., Kaiser, J.F. (ed.) (1993). *Handbook for Digital Signal Processing*, Wiley.

[5] Zygarlicki, J., Zygarlicka, M., Mroczka, J., Latawiec, K.J. (2010). A reduced Prony's method in power-quality analysis-parameters selection, *IEEE Trans. Power Del.*, 25(2), 979-986.

[6] Renders, H., Schoukens, J., Vilain, G. (1984). High-Accuracy Spectrum Analysis of Sampled Discrete Frequency Signals by Analytical Leakage Compensation, *IEEE Trans. Instrum. Meas.*, 33(4), 287-292.

[7] Zakharov, Y.V., Tozer, T.C. (1999). Frequency estimator with dichotomous search of periodogram peak, *Electronics Letters*, 35(19), 1608-1609.

[8] Reisenfeld, S., Aboutanios, E. (2003). A New Algorithm for the Estimation of the Frequency of a Complex Exponential in Additive Gaussian Noise, *IEEE Communications Letters*, 7(11), 549-551.

[9] Aboutanios, E., Mulgrew, B. (2005). Iterative Frequency Estimation by Interpolation on Fourier Coefficients, *IEEE Transactions on Signal Processing*, 53(4), 1237-1242.

Metrol. Meas. Syst., Vol. XVIII (2011), No. 3, pp. 391-402.

[10] He, B., Cabestaing, F., Postaire, J.G., Zhang, R. (2005). Narrow-Band Frequency Analysis for Laser-Based Glass Thickness Measurement, *IEEE Transactions on Instrumentation and Measurements*, 54(1), 222-227.

[11] Zivanovic, M., Carlosena, A. (2001). Nonparametric Spectrum Interpolation Methods: A Comparative Study, *IEEE Transactions on Instrumentation and Measurement*, 50(5), 1127-1132.

[12] Zivanovic, M., Carlosena, A. (2002). Extending the limits of resolution for narrow-band harmonic and modal analysis: a non-parametric approach, *Measurement Science and Technology*, 13(12), 2082-2089.

[13] Porat, B. (1996). *A Course in Digital Signal Processing*, Wiley.

[14] Rabiner, L.R., Schafer, R.W., Rader, C.M. (1969). The chirp-z transform algorithm, *IEEE Trans. on Audio and Electroacoustics*, 17(2), 86-92.

[15] Aiello, M., Cataliotti, A., Nuccio, S. (2005). A Chirp-Z Transform-Based Synchronizer for Power System Measurements, *IEEE Transactions on Instrumentation and Measurement*, 54(3), 1025-1032.

[16] Sarkar, I., Fam, A.T. (2006). The interlaced chirp Z transform, Signal Processing, 86, 2221-2232.

[17] Duda, K., Borkowski, D., Bień, A. (2009). Computation of the network harmonic impedance with Chirp-Z transform, *Metrology and Measurement Systems*, 16(2), 299-312.

[18] Makur, A., Mitra, S.K. (2001). Warped Discrete-Fourier Transform: Theory and Applications, *IEEE Transactions on Circuits and Systems – I: Fundamental Theory and Applications*, 48(9), 1086-1093.

[19] Franz, S.F., Mitra, S.K., Doblinger, G. (2003). Frequency estimation using warped discrete Fourier transform, *Signal Processing*, 83, 1661-1671.

[20] Venkataramanan, R., Prabhu, K.M.M. (2006). Estimation of frequency offset using warped discrete-Fourier transform, *Signal Processing*, 86, 250-256.

[21] Rife, D.C., Vincent, G.A. (1970). Use of the Discrete Fourier Transform in the Measurement of Frequencies and Levels of Tones, *Bell System Technical Journal*, 49, 197-228.

[22] Kamm, G.N. (1978). Computer Fourier-transform techniques for precise spectrum measurements of oscillatory data with application to the de Haas-van Alphen effect, *J. of App. Phys.*, 49(12), 5951-5970.

[23] Jain, V.K., Collins, W.L., Davis, D.C. (1979). High-Accuracy Analog Measurements via Interpolated FFT, *IEEE Transactions on Instrumentation and Measurements*, 28(2), 113-121.

[24] Grandke, T. (1983). Interpolation Algorithms for Discrete Fourier Transforms of Weighted Signals, *IEEE Transactions on Instrumentation and Measurement*, 32, 350-355.

[25] Andria, G., Savino, M., Trotta, A. (1989). Windows and Interpolation Algorithms to Improve Electrical Measurement Accuracy, *IEEE Transactions on Instrumentation and Measurement*, 38(4), 856-863.

[26] Offelli, C., Petri, D. (1990). Interpolation Techniques for Real-Time Multifrequency waveform analysis, *IEEE Transactions on Instrumentation and Measurement*, 39(1), 106-111.

[27] Schoukens, J., Pintelon, R., Van Hamme, H. (1992). The Interpolated Fast Fourier Transform: A Comparative Study, *IEEE Transactions on Instrumentation and Measurement*, 41(2), 226-232.

[28] Quinn, B.G. (1994). Estimating Frequency by Interpolation Using Fourier Coefficients, *IEEE Transactions on Signal Processing*, 42(5), 1264-1268.

[29] Quinn, B.G. (1997). Estimating of Frequency, Amplitude, and Phase from the DFT of a Time Series, *IEEE Transactions on Signal Processing*, 45(3), 814-817.

[30] Macleod, M.D. (1998). Fast Nearly ML Estimation of the Parameters of Real or Complex Single Tones or Resolved Multiple Tones, *IEEE Transactions on Signal Processing*, 46(1), 141-148.

[31] Sedlacek, M., Titera, M. (1998). Interpolations in frequency and time domains used in FFT spectrum analysis, *Measurement*, 23, 185-193.

[32] Santamaria, I., Pantaleon, C., Ibanez, J. (2000). A Comparative Study of High-Accuracy Frequency Estimation Methods, *Mechanical Systems and Signal Processing*, 14(5), 819-834.

[33] Borkowski, J. (2000). LIDFT – the DFT linear interpolation method, *IEEE Trans. Instrum. Meas.*, 49(4), 741-745.

[34] Borkowski, J., Mroczka, J. (2000). Application of the discrete Fourier transform linear interpolation method in the measurement of volume scattering function at small angle, *Optical Eng.*, 39(6), 1576-1586.

[35] Borkowski, J., Mroczka, J. (2002). Metrological analysis of the LIDFT method, *IEEE Transactions on Instrumentation and Measurement*, 51(1), 67-71.

[36] Agrež, D. (2002). Weighted Multipoint Interpolated DFT to Improve Amplitude Estimation of Multifrequency Signal, *IEEE Transactions on Instrumentation and Measurement*, 51(2), 287-292.

[37] Liguori, C., Paolillo, A. (2007). IFFTC-Based Procedure for Hidden Tone Detection, *IEEE Transactions on Instrumentation and Measurements,* 56(1), 133-139.

[38] Belega, D., Dallet, D. (2008). Frequency estimation via weighted multipoint interpolated DFT, *IET Science, Measurement and Technology*, 2(1), 1-8.

[39] Chen, K.F., Li, Y.F. (2008). Combining the Hanning windowed interpolated FFT in both directions, *Computer Physics Communications*, 178, 924-928.

[40] Li, Y.F., Chen, K.F. (2008). Eliminating the picket fence effect of the fast Fourier transform, *Computer Physics Communications*, 178, 486-491.

[41] Belega, D., Dallet, D. (2009). Multifrequency signal analysis by Interpolated DFT method with maximum sidelobe decay windows, *Measurement*, 42, 420-426.

[42] Yang, X.Z., Li, H.Y., Chen, K.F. (2009). Optimally averaging the interpolated fast Fourier transform in both directions, *IET Science, Measurement and Technology*, 3(2), 137-147.

[43] Chen, K.F., Jiang, J.T., Crowsen, S. (2009). Against the long-range spectral leakage of the cosine window family, *Computer Physics Communications*, 180, 904-911.

[44] Chen, K.F., Mei, S.L. (2010). Composite Interpolated Fast Fourier Transform With the Hanning Window, *IEEE Transactions on Instrumentation and Measurement*, 59(6), 1571-1579.

[45] Borkowski, J., Mroczka, J. (2010). LIDFT method with classic data windows and zero padding in multifrequency signal analysis, *Measurement*, 43, 1595-1602.

[46] Duda, K. (2010). DFT Interpolation Algorithm for Kaiser–Bessel and Dolph–Chebyshev Windows, *IEEE Transactions on Instrumentation and Measurement*, 60(3), 784-790.

[47] Harris, F.J. (1978). On the use of windows for harmonic analysis with the Discrete Fourier Transform, *Proceedings of the IEEE*, 66(1), 51-83.

[48] Mroczka, J., Szczuczyński, D. (2009). Inverse problems formulated in terms of first-kind Fredholm integral equations in indirect measurements, *Metrology and Measurement Systems*, 16 (3), 333-357.

[49] Szmajda, M, Górecki, K, Mroczka, J. (2010). Gabor transform, spwvd, gabor-wigner transform and wavelet transform - tools for power quality monitoring, *Metrology and Measurement Systems*, 17(3), 383-396.